Received 16 April 2022; accepted 8 May 2022. Date of publication 13 May 2022; date of current version 25 May 2022.

Digital Object Identifier 10.1109/OJCOMS.2022.3174893

Robust Resource Allocation for Indoor Self-Blockage Millimeter Wave Device-to-Device Communications

HAIE DOU, XIAOTING YU, BIN KANG, MINGKAI CHEN (Member, IEEE), LEI WANG (Member, IEEE), AND BAOYU ZHENG (Senior Member, IEEE)

Key Laboratory of Broadband Wireless Communication and Sensor Network Technology, Nanjing University of Posts and Telecommunications, Ministry of Education, Nanjing 210003, China

CORRESPONDING AUTHOR: L. WANG (e-mail: wanglei@njupt.edu.cn)

This work was supported in part by The National Natural Science Foundation of China under Grant 62071255, Grant 62001246, Grant 62171232, Grant 61771257, and Grant 61671253; in part by The Major Projects of the Natural Science Foundation of the Jiangsu Higher Education Institutions under Grant 20KJA510009; in part by the China Postdoctoral Science Foundation under Grant 2020M681684; and in part by the Jiangsu Postdoctoral Science Foundation under Grant 2021K278B.

ABSTRACT The advancement of millimeter wave (mmWave) technology can meet the requirements of large amounts of data communications among intelligent devices for indoor scenarios. However, reducing interference in an enclosed region is still challenging because the human body becomes the main blockage in indoor scenarios. In this paper we develop a robust system to exploit the self-blockage model for analysing the side effect of the human body and adopting a multi-ball Line of Sight (LOS) link state model to describe the conventional blockage. The combination of self-blockage and link state models will provide a more comprehensive and accurate expression for indoor obstacles that disturb the communication robustness. Besides, we formulate the resource allocation as a robust optimization problem, where the proposed optimization function is to achieve the maximum throughput by minimizing interference. We have given a closed expression of coverage rate to analyze the system performance. The simulation results show that the proposed model can accurately describe the distribution of blockages for indoor cases.

INDEX TERMS mmWave, device-to-device communications, resource allocation, vertex coloring algorithm.

I. INTRODUCTION

RECENTLY, the indoor communications among devices in an enclosed space have attracted more attention. With the development of mobile devices (e.g., smartphones, tablets) and corresponding applications, it is urgent to improve data rate and the robustness of the indoor communications [1], [2]. Specifically, as an offloading traffic approach, physical proximity device communication based device-to-device (D2D) communication in indoor scenarios reuses the resources to improve system throughput drastically [3], [4]. This will yield high capacity, high security and seamless transmission in the future [5], [6], [7]. Due to the huge bandwidth available in 60 GHz, mobile devices with D2D communication strategy can achieve multi-gigabit communication services [8], [9]. Although introducing mmWave technology in D2D communication could effectively raise the total system throughput, the severe channel fading problem still exists. To reduce pass loss, high gain directional antennas are exploited on mobile devices to obtain high precise transmission in [10], [11], [12], [29], [30], [31], intelligently aligning the main beams and nullifying the orientation of interference.

In fact, the capacity of indoor communication is not only related to system bandwidth, but also to the density of devices and distribution of obstructions. Thus, the locations of the obstacles or base stations were modeled as Poisson point process (PPP) [13], [14], [15]. As the density of blockage is vital to the success of D2D transmission, literatures [16] and [17] introduced a three-state path-loss, including Line of Sight (LOS), non-Line-of-Sight (NLOS) and outage links to overcome obstacles. In particular, a two-objective optimization problem is proposed

in [16] to optimize the user association of millimeter wave support base stations. After [16] and [17], the works [18] and [19] proposed to mix precoding and power distribution for obtaining optimal transmit antenna selection and channel assignment. Subsequently, authors in [20] proposed a new self-organizing network to characterize relay networks. This network did not define mmWave specific features (e.g., directional antennas, blockage) clarify. In [21], [22], [23], the scene was moved into an enclosed area where the human body is considered as the main blockage. The limitation of [21], [22], [23] was that they did not take reflections from the ceiling and walls into consideration. In [24], the ceilings could highly reflect the signal, leading to less blocked transmission. Moreover, a closed form expression for interference plus noise ratio (SINR) was not given [24].

After the above review on indoor blockage and interference models, credible resource allocation has become the key point in D2D oriented indoor communications. For credible resource allocation, a cluster-based intelligent IoT scheme is proposed in [25], which is based on the perception and transmission performance of the intelligent IoTs. Besides of [25], vertex-coloring was used to obtain higher throughput in [26]. The limitation of [26] was that it was required to recompute weights after coloring enhances the complexity. Aforementioned works have made eminent achievement in blockage modeling and resource allocation respectively. However, they cannot apply the allocation scheme to the practical blockage case.

For indoor resource allocation with a simplified model, the main contributions of this paper are three folds. First, by combining multi LOS ball link with self-blockage model [27], [28], we improve the interference and blockage model to describe the distribution of obstacles. Second, we derive a closed expression of SINR coverage probability characterized by body orientation and location, which is helpful for analyzing system performance. Third, we formulate the resource allocation as a robust oriented optimization problem and give an expression to maximize throughput under the condition of the proposed model. Since the proposed optimization problem under huge interference is a NP-hard problem. For valid counteraction, a new PMVC scheme is proposed to deal with interference and increase the total throughput. We carry out extensive experiments to show that the throughput is improved evenly.

The rest of this paper is organized as follows. The system model is introduced in Section II. In Section III, we establish a SINR model, using a closed expression to analyse coverage probability. Moreover, we illustrate the theoretical results with Monte Carlo simulations to depict coverage probability as SINR moves down. The indoor conditions and new PMVC scheme are shown in Section IV. Numerical results of PMVC comparing to other algorithms are given in Section V. Finally, conclusions and future work are given in Section VI.

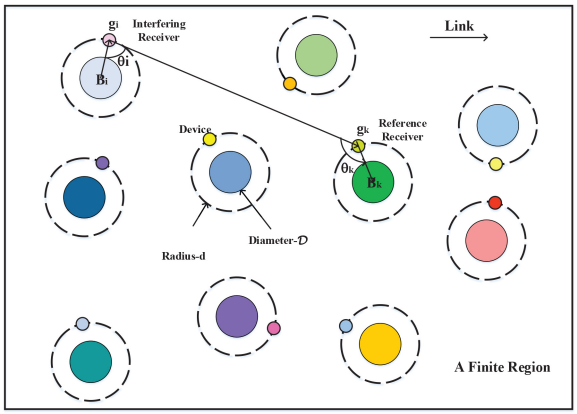

FIGURE 1. An illustration of orbital models with the blockages randomly distributed in a finite region, facing g_k with θ_j and facing g_j with θ_j.

II. SYSTEM MODEL

A smart indoor network is considered, where mobile devices equipped with directional-antennas serve as transmitters or receivers. The directional-antenna is characterized by its main lobe towards the cardinal propagation while the other side lobes disperse the energy. Compared with traditional omni-directional antenna, the adaptive directional-antenna brings the decrease in the additional noise caused by large transmission bandwidth. Meanwhile, it also remedies the increased path-loss at mmWave frequencies. Combined with network geometry, the blockage and interference model is discussed below.

A. NETWORK MODEL

Defining an infinite region Υ with a reference device pair and several interfering transmitters. The users located in Υ are subject to a PPP with the density λ. These locations are denoted by g_k. Further, the interferers can be expressed by the same way g_i, under a distance of R_i. As it is shown in Fig. 1, we assume that each blockage, including human body, is settled to be a circle with the diameter of $\mathcal{D}$. The obstructions associated with the reference transmitter are denoted by B_k, whose azimuth angle to g_i is θ_k. Similarly, the definition of blockage, which is related to interfering nodes, as B_i, facing g_k with angle θ_i.

Assumption 1: To further explore the relations between blockages and interferers, the ring model is utilized to describe the locations of obstacles. When the user holds a mobile device in hand, the transmitter or receiver is bounded to distribute around himself. As the planar graph looks like a ring in Fig. 1, we consider it as a ring model. Hence, we position the g_k randomly on a circle with radius $d > \frac{\mathcal{D}}{2}$ centering the B_k. It is clear that the ring model is a valued and inherent part of the self-blockage where body orientation weighs heavily.

B. SIGNAL MODEL

As each device is equipped with a directional antenna, the directional beamforming is exploited to steer beams. The

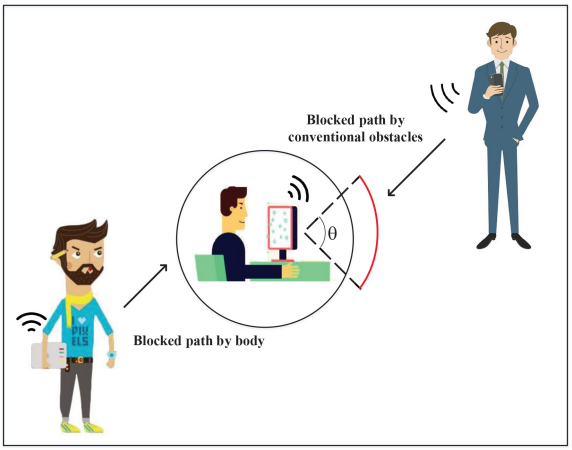

FIGURE 2. Illustration of a blocking cone showing the signal paths blocked by human body and conventional obstacles respectively under a condition of indoor case.

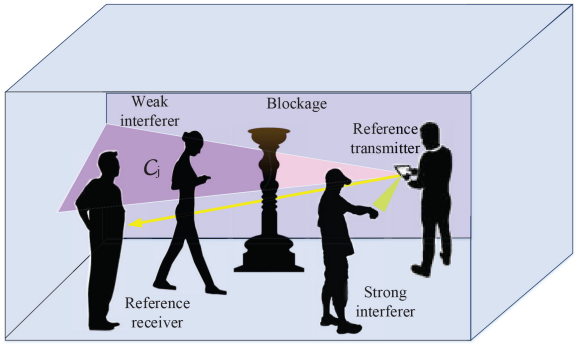

FIGURE 3. In an indoor finite region a blocking zone stretched from Fig. 1 is exhibited.

antenna gain G characterized by: main beamiwdth θ', main lobe gain (G_f) and back lobe gain(G_b) is denoted by:

$$G = \begin{cases} G_f G_f & \text{w.p.} \left(\frac{\theta'}{\pi}\right)^2 \\ G_f G_b & \text{w.p.} 2\left(\frac{\theta'}{\pi}\right)\left(\frac{\pi-\theta'}{\pi}\right) \\ G_b G_b & \text{w.p.} \left(\frac{\pi-\theta'}{\pi}\right)^2. \end{cases} \tag{1}$$

We assume that the antenna gain is $G_f G_f$ under the conditions of perfect alignment of the transmitting main lobe and receiving main lobe in the formula above, with probability $(\frac{\theta'}{\pi})^2$. Similarly, if the transmitting main lobe is biased to receiving the back lobe, the gain $G_b G_b$ appears with probability $(\frac{\pi-\theta'}{\pi})^2$. Since there are two cases where the main lobe is shifted to back lobe, the gain $G_f G_b$ occurs in a probability $2(\frac{\theta'}{\pi})(\frac{\pi-\theta'}{\pi})$.

C. BLOCKAGE AND INTERFERENCE MODEL

The transmission link is defined as either LOS or NLOS. Owing to the high attenuation of mmWave, the link state totally depends on the indoor environment, where blockages scatter all around. Besides the conventional obstacles, the human bodies are the primary blockages for indoor mmWave communications. During transmission between typical reference pairs, g_k is not only blocked by B_i, but also much possible blocked by its own correlative blockage B_k. In other words, there is an even greater likelihood that the transmission link is blocked by the user himself, called self-blockage, which is related to whether g_k are straightly facing g_i.

Due to the special indoor mmWave situation, the two assumptions in the following are given for better illustration of key ideas in Fig. 2.

Assumption 2: When the transmission link falls into a determined cone of angle in space, self-body human blockages happen, as shown in Fig. 2. The parameter θ is defined as the blocking angle, which is relevant to the width of the human body and its position. Under the assumption that each transmission link path is identically and independently distributed, they arrive with a fixed chance $j_r = \frac{\theta}{2\pi}$. The constant signal attenuation across the cone is defined in advance. If the signal path drops into the angle of blockage cone, there will be an attenuation in received power expressed by a constant factor $\mathcal{F}$. When $\mathcal{F}$ is close to zero, the system is much simplified.

Assumption 3: The location of the blockages is still subject to independent point processes. There are two kinds of blockages presumed in this finite region, which include common obstacles and human body obstructions. That is to say, the communication link would be blocked by conventional blockages or more likely human bodies.

For *Assumption 3*, except for B_i and B_k, we assume the signal link also could be blocked by $B_j, j \neq i$. The distinct difference between the self-blockage and these ordinary blockages is whether it depends on the locations of g_k and g_i. Actually, the self-blockage happens while g_k are not facing towards g_i. For example, if a user turns his back to the arrival link, the transmission will absolutely be blocked. However, the ordinary blockage has no limited restrictions. Accordingly, this assumption would occur when no signal link is self-blockage and these two cases should be discussed separately.

Assumption 4: Small-scale fading can be obviously neglected for small-scale fading results in an ignorable impact. The received power is hardly affected while the directional antennas are used in mmWave indoor case. In addition, Nakagami fading is independent for each link, so that small-scale fading is common to mention. To reduce the complexity, we ignore the changes in channel response, as well as frequency selection.

If there are blocks $B_j, j \neq i$ absent from reference transmitters, we assume it is strong interference and g_i is defined as strong interferer. Otherwise, the link is noted as weak interference with g_i. As it is shown in Fig. 3, on the condition of being no self-blockages during the transmission link, once g_i is blocked by B_j, the area $\mathcal{C}_j$ is assumed to be the blocking zone where any users could not obtain successful transmission. When $g_i \in \mathcal{C}_j$, g_i is a weak interference. And

a blocking zone shown in Fig. 3 is given.

$$\mathcal{C}_j = \left\{ \begin{array}{l} g_i \in \Upsilon : \frac{\mathcal{D}}{2} < \left| g_i - B_j \right| \\ \leq \frac{\mathcal{D}}{4} \sin^{-1} \frac{\theta_k}{2}, \forall j \neq i \end{array} \right\} \tag{2}$$

Under this assumption, if g_i is a weak interference, it is more likely that there exist blocks between reference pairs. There are S different states assumed to define the blockage model, which include LOS and NLOS. Accordingly, we exploit the multi LOS ball link state and further describe the distribution of indoor obstacles $B_j, j \neq i$. The distance from the reference transmitter to reference receiver is divided into C number of LOS link balls from near to far, in order to judge whether $B_j, j \neq i$ belongs to this ball. As the radius increases, the ball is approaching the reference receiver. Once $B_j, j \neq i$ exists in the ball, the link to be NLOS, means a failure in transmission; otherwise the link to be LOS, requires further verification. The $P_s(\cdot)$ is noted as the probability of the node's being in state, calculated as:

$$P_s(r) = \sum_{c=1}^{C+1} q_s^{[D_{c-1}, D_c]} 1_{[D_{c-1}, D_c]}(r), \tag{3}$$

where $\sum_{s \in S} p_s(r) = 1$ and C indicate the number of circles. When $D_0 = 0$ and $D_{c+1} = +\infty$ are predetermined, D_c is supposed to be the radius of the circle C. Define an indicator function $1_{[D_{c-1}, D_c]}(r)$ to judge whether r belongs to $[x, y)$, which returns unity if $r \in [x, y)$; 0 otherwise. The probability $q_s^{[D_{c-1}, D_c]}$ implies the link in state S when $r \in [D_{c-1}, D_c)$.

$$\sum_{s \in S} q_s^{[D_0, D_1]}(r) = \cdots = \sum_{s \in S} q_s^{[D_{c-1}, D_c]}(r) = 1. \tag{4}$$

It is obvious that the more the ball exists, the higher the accuracy of the model is. However, as B_j increases, the complexity of analysis also increases. In order to get a balance between these two factors, as shown in Eq. (4), a three-ball approximation is defined here. The multiple ball approximation in Eq. (4) can be considered as an expansion of a single LOS ball. We decompose Eq. (3) into Eq. (4) where $D_3 > D_2 > D_1 > 0$. As the radius D_c can arbitrarily be any value, the regions emerge for LOS state with different probability. With Υ divided into four regions, we need to approximate the mean link probabilities of different states in Eq. (4). The LOS link is finally computed as $p_L(r) = \min\{\mathcal{G}/r\}(1 - e^{(-\frac{r}{2\mathcal{G}})}) + e^{(-\frac{r}{2\mathcal{G}})}$, where $\mathcal{G}$ is correlative to the range and the situation of the enclosed region Υ. So that we can easily obtain the probability of link in NLOS, denoted as $p_N(r) = 1 - p_L(r)$. And the second equation in Eq. (4) is an approximation constraint which ensures that the state of these regions is either LOS or NLOS.

Further, in order to determine if there exists $B_j, j \neq i$, a region $\Im$ is given. Since $B_j, j \neq i$ also defers to PPP, the probability of no user in region $\mathcal{C}_j$ is expressed as $e^{-\lambda|\Im|}$. As illustrated in Fig. 4, the actual area of $\Im$ is approximated by:

$$\Im = \frac{\pi D_c^2}{2}. \tag{5}$$

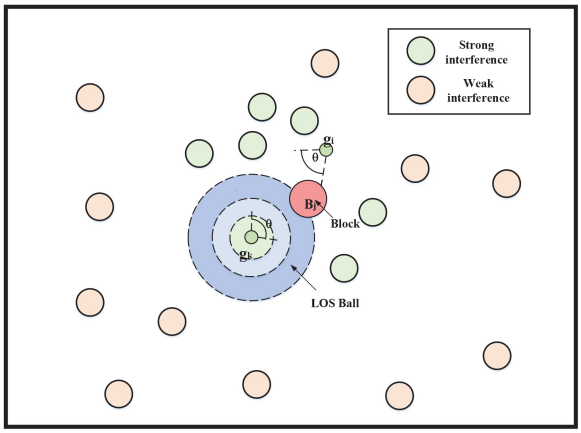

FIGURE 4. Plot showing blocking region B_j with the fixed threshold R_B accompanied with strong interference and weak interference scattering all around. The LOS link balls from the near to far to verify whether this is a LOS link.

With the limits of Eq. (5), the probability that there is any user in $\Im$, is obtained by:

$$p_b(g_k) = 1 - e^{-\lambda\left(\frac{\pi D_c^2}{2}\right)}. \tag{6}$$

The distance between the interferer and the reference receiver is random. The longer the distance is, the higher the probability of the block $B_j, j \neq i$ exits. The threshold value R_B is to give a judgement on whether the transmission path is blocked. Whenever the probability $p_b(g_k)$ is achieved, the threshold value R_B is determined. This is calculated by preserving the average numbers of strong interferers. As once a link is blocked, obviously the interference is weak and we need to abandon it. Instead, we hold the average number of strong interferers with the expression

$$\begin{aligned} \rho(g_k) &= E\left[\sum_{g_k \in \Upsilon} I_\phi^W \right] \\ &= 2\pi\lambda \int_{g_k \in \Upsilon} (1 - p_b(g_k)) g_k dg_k \\ &= 2\left(1 - e^{-\frac{\pi\lambda D_c^2}{2}}\right). \end{aligned} \tag{7}$$

As the mean number of interferers in a threshold of radius R_B is $\lambda\pi R_B^2$, the value of radius reference to Eq. (7) is

$$R_B = \left[\frac{\rho(g_k)}{\lambda\pi} \right]^{0.5}. \tag{8}$$

III. SINR ANALYSIS OF COVERAGE PROBABILITY

The SINR seen from receiver is denoted by

$$SINR = \frac{P_t M_0 h_0 r^{-\alpha_L}}{\sigma^2 + \sum_{i \in \Phi} P_t M_0 h_i l(r)}, \tag{9}$$

where P_t is transmit power and M_0 is the antenna gain related to alignment of both main beams. Due to Nakagami fading being used, both h_0 and h_i are defined as normalized Gamma functions with random variable N. And the noise power delivered by the reference transmitter is denoted as σ^2.

A. COVERAGE PROBABILITY

A coverage probability denoted by β is given when the complementary cumulative distribution function (CCDF) of SINR is greater than a threshold

$$P_c = \{\beta \geq \gamma\}. \tag{10}$$

Plugging the quantities in Eq. (10), and rearranging it leads to:

$$\begin{aligned} P_c &= \mathrm{P}\left\{\frac{P_t M_0 h_0 r^{-\alpha_0}}{\sigma^2 + \sum_{i\in\Phi} P_t M_i h_i d_i^{-\alpha_i}} \geq \gamma\right\} \\ &= \mathrm{P}\left\{h_0 \geq \frac{\gamma r^{\alpha_0}}{P_t M_0}\left(\sigma^2 + \sum_{i\in\Phi}\frac{P_t M_i h_i}{d_i^{\alpha_i}}\right)\right\} \\ &= \mathrm{P}\left\{h_0 \geq \frac{\gamma r^{\alpha_0}}{P_t M_0}\left(\sigma^2 + I_\Phi\right)\right\}, \end{aligned} \tag{11}$$

where $I_\Phi = I_\Phi^W + I_\Phi^S$ indicates the summation of the strong interference and weak interference. Under the circumstance of self-blockage, the effects brought by strong interferer are largely debased. However, due to the self-blockage, a signal with a weak interferer is exposed to a more weakened link state. The LOS or NLOS signal link is decorated with a pass-loss exponent α_L or α_N respectively, and $\alpha_N > \alpha_L$. As the number of self-blockages is predetermined, the path-loss reference to the features of LOS/NLOS is as follows:

$$l(r) = \begin{cases} |r|^{-\alpha_L} B_L^{-s} \\ |r|^{-\alpha_N} \end{cases} \tag{12}$$

where the upper one occurs if there is a strong interferer, and the other one utilizes an indicator function to distinguish the condition of strong interferers. Actually, experiencing a weak interferer, some diffractions and scatterings in Υ are still inevitable. Equation (11) could be further expressed as:

$$\begin{aligned} P_c &= \mathrm{P}\left\{h_0 \geq \frac{\gamma r^{\alpha_0}}{P_t M_0}\left(\sigma^2 + I_\Phi\right)\right\} \\ &= 1 - E\left[\left(1 - e^{-\overline{\eta\gamma}\left(\sigma^2 + \sum_{i\in\Phi} P_t M_i h_i l(r)\right)}\right)^N\right]. \end{aligned} \tag{13}$$

If we presume ∂ to be a normalized gamma random variable and a constant $\Theta > 0$, the upper bound of the probability is $P(\partial < \Theta) < \left[1 - e^{-\overline{\eta}\Theta}\right]$. Besides, N is the parameter of the gamma fading. Hence $\overline{\eta} = N(N!)^{-\frac{1}{N}}$ is a gamma random variable used to evaluate CDF. Meanwhile, $\overline{\gamma} = \frac{\gamma r_0^{\alpha_L}}{P_t M_0}$ needs to be plugged into the formula above. By using binomial distribution, a new approximation can be obtained:

$$\begin{aligned} P_c \approx \sum_{n=1}^{N} (-1)^{n+1}\binom{N}{n} e^{-kN(N!)^{\frac{-1}{N}}\overline{\gamma}\sigma^2} \\ \times\ E_\Phi\left[e^{-kN(N!)^{\frac{-1}{N}}\overline{\gamma} I_\Phi^S}\right] E_\Phi\left[e^{-kN(N!)^{\frac{-1}{N}}\overline{\gamma} I_\Phi^W}\right]. \end{aligned} \tag{14}$$

With the R_B computed in Eq. (8), the Laplace transformation of the LOS and NLOS fields are denoted by:

$$\begin{aligned} &E_\Phi\left[e^{-k\overline{\eta\gamma} I_\Phi^S}\right] \\ &= E_N\left[E_{g_i\in \mathrm{C}j}\left[(1-q_s) + q_s\left[j_{\mathrm{r}}\wp^{-N} + (1-j_{\mathrm{r}})\wp^{-N}\right]\right]\right] \\ &= E_N\left[2\int_0^{D_c}\left[(1-q_s)R_B^{-2} + \sum_{k=1}^{4} j_{\mathrm{r}_k} q_s \wp^{-N}\right]\frac{r}{R_B^2}dr\right] \\ &= e^{-2\pi\lambda q_s\left(\frac{D_c^2}{2} - \int_0^{D_c}\sum_{k=1}^{4} j_{\mathrm{r}_k}\wp^{-N}\right)}, \end{aligned} \tag{15}$$

$$\begin{aligned} &E_\Phi\left[e^{-k\overline{\eta\gamma} I_\Phi^W}\right] \\ &= E_N\left[E_{g_i\in\Upsilon/\mathrm{C}j}\left[\prod_{i=1}^{N}\wp^{-N}\right]\right] \\ &= e^{-\lambda\left(\kappa\sin^{-1}\left(1-\frac{\mathcal{D}^2}{4d^2}\right)^{0.5}\mathcal{Z}_1 + \left(1-\kappa\sin^{-1}\left(1-\frac{\mathcal{D}^2}{4d^2}\right)^{0.5}\mathcal{Z}_2\right)\right)}, \end{aligned} \tag{16}$$

where $\wp = 1 + lk\overline{\eta\gamma}G$ and G exactly depict the configuration of each antenna beam direction, related to the antenna gain Eq. (1). To achieve expected terms of strong interference and weak interference, we assume $\mathcal{P}$ number of strong interferers and $\mathcal{M}$ number of weak interferers respectively. Thus, the $\mathcal{P}$ and $\mathcal{M}$ interferers are Poisson distributed with mean $\lambda\pi R_B^2$ and $\lambda|\Upsilon - \frac{\pi\mathcal{D}^2}{4}|$. Besides, the distance between strong interferer and reference receiver is subject to the distribution $f(r) = \frac{2r}{R_B^2}$. We will obtain the two notations with probability of falling into block zone and not falling into block zone. By averaging over $\mathcal{P}$ interferers, the strong interference expectation is computed in Eq. (15). Similarly, it is available under the weak interference.

We add the path-loss formula for an exact expression with

$$\mathcal{Z}_1 = |\upsilon| - \int\left(1 + \frac{k\overline{\eta\gamma}}{(|r|)^{-\alpha_L}}\right)dr. \tag{17}$$

and

$$\mathcal{Z}_2 = |\upsilon| - \int\left(1 + \frac{k\overline{\eta\gamma}}{(|r|)^{-\alpha_N}}\right)^{-N}dr. \tag{18}$$

Each Laplace transformation is simply calculated, except for κ, where $\kappa = \frac{4\mathrm{C}_j - \pi D_c^2}{4\Upsilon - \pi D_c^2}$ depends on antenna gain. The averaged SINR coverage probability can be calculated by adding Eq. (15) and Eq. (16) into Eq. (14). For better transmission capacity, we are urgent to capture the largest λ which can be easily achieved by presetting the SINR threshold and outage χ. It is apparent that once $1 - \chi$ appears, the SINR, larger than a threshold, would be received. To achieve this inequality, the distribution of the SINR can be approximated by:

$$\begin{aligned} P_c &\approx \sum_{n=1}^{N}(-1)^{n+1}\binom{N}{n}\left[1 - \lambda\varsigma + \lambda^2\varsigma^2\right] \\ &and \begin{cases} \varsigma = 2\pi U + V \\ U = q_s\left(\frac{D_c^2}{2} - \int_0^{D_c}\sum_{k=1}^{4} j_{\mathrm{r}_k}\wp^{-N}\right) \\ V = \kappa\mathcal{Q}\mathcal{Z}_1 + (1 - \kappa\mathcal{Q}\mathcal{Z}_2) \\ \mathcal{Q} = \sin^{-1}\left(1 - \frac{\mathcal{D}^2}{4d^2}\right)^{0.5}. \end{cases} \end{aligned} \tag{19}$$

We use $e^x \approx 1 + x + \frac{x^2}{2}$ to approximate Eq. (15), (16), when P_c closes 1. Actually, U and V are related to the LOS and NLOS interference respectively. In addition, both

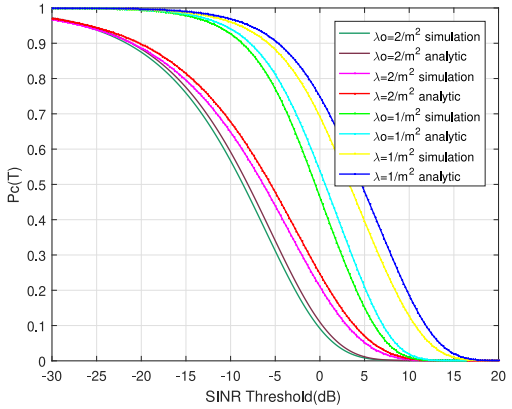

FIGURE 5. SINR coverage rate obtained through comparison between Monte Carlo simulation and analytic expression when $\lambda = 1$ and $\lambda = 2$.

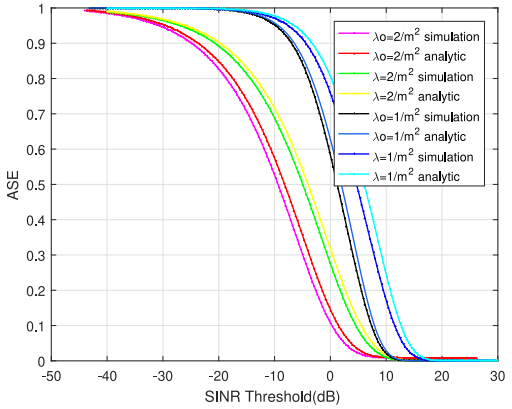

FIGURE 6. CCDF of spectral efficiency when $\lambda = 1$ and $\lambda = 2$ respectively under the comparison between Monte Carlo simulations and analytic results.

U and V can be decomposed further based on gains received from each antenna. In the first equation, the noise, LOS interference and NLOS interference are related to exponential terms. Thus, we can respectively compare the single relative contribution with the total SINR CCDF.

Primarily, as SINR changes we present the coverage probability, to show the benefits of the model. With the empirical data given by $\lambda = 1$ and $\lambda = 2$, the Fig. 5 exhibits SINR distributions between the self-blockage model and the proposed model. First of all, the errors of the approximation are small. It proves that the performance of the system is much more accurate due to the directional antennas and predetermined threshold value R_B. Actually, with higher density, the reference transmitter is of more risk to experience interferer scattering around. It is clear that the performance of the combined model is better than the original model via comparison.

B. AREA SPECTRAL EFFICIENCY

Area spectral efficiency is the significant metric to evaluate system performance because it can scrutinize the network condition. SINR is denoted by Γ, the spectral efficiency per channel is

$$\eta = W_k \log_2(1 + \Gamma) \tag{20}$$

where W_k is system bandwidth. It is clear that ASE can be obtained through the Monte Carlo simulations and analytical expressions. We can obtain the average spectral efficiency by simulations. Since the interferer randomly distributed in the scenario, we preset a fixed number of interference drawn from a binomial point process (BPP). When a large group of channel realizations is generated, the correlative ASE for each position could be computed exactly. In virtue of the high accuracy, calculations needed to be repeated, to obtain the spatial average. With the limit of an infinite number of trials, this method approaches the precise mean performance nearly. However, the complexity is too high. In contrast, the analytical result just requires to take Rayleigh fading into consideration for the links. The spatially outage probability should be predetermined by measuring the positions of the interferers and the blockages. By confirming the density of interferers and obstacles, we find spatially averaged outage probability. Through this approach, we can easily obtain a closed-form expression for the CCDF of the ASE. According to Eq. (20), if $\eta < W_k \log_2(1 + \Gamma)$, we can compute the CCDF spectral efficiency as:

$$\begin{aligned} P_\eta[SINR > \eta] &\to P_c\left[SINR > 2^{\frac{\eta}{W_k}} - 1\right] \\ &= P_c\left(2^{\frac{\eta}{W_k}} - 1\right). \end{aligned} \tag{21}$$

If $X \geq 0, E[X] = \int_0^\infty (1 - F(x))dx$, the area spectral efficiency could be expressed as:

$$E[\eta] = \frac{W_k}{\ln 2} \int_0^\infty \frac{P_c}{1 + \Gamma} d\Gamma, \tag{22}$$

where $d\eta = d\Gamma / 1n2(1 + \Gamma)$ varies with $\Gamma = 2^{\eta / W_k} - 1$.

There is a maximum rate and a minimum rate given by $\beta_{\max}$ and $\beta_{\min}$ during the practice. The modulation order of the distortion and constellation limits in the radio frequency may directly affect the maximum rate while the high receiver sensitivity influences the minimum rate. As a result, Eq. (22) can be further expressed as:

$$E[\eta] = \frac{W_k}{\ln 2} \int_{\beta_{\min}}^{\beta_{\max}} \frac{P_c}{1 + \Gamma} d\Gamma. \tag{23}$$

By averaging the human locations and body orientations, we can easily obtain closed-form expression for CCDF of the ASE with different user density. The proposed model and original model are then validated against the results obtained via comparison between analyses and simulations shown in Fig. 6. It is clear that the proposed model achieves better performance than the self-blockage model.

C. OPTIMIZATION OF VERTEX COLORING ALGORITHM

Once blockage modeling is completed, multiple links can achieve transmition simultaneously in such intensive scenarios, which may cause serious interference between links and affect high-speed transmission performance. Therefore, how

to design an effective resource allocation algorithm to reduce the interference and improve the network throughput is an urgent question.

Under the blockage and interference model discussed above, in the following, we illustrate the data transmission for indoor D2D communications in 60 GHz network. In this scenario, the focus on indoor resource allocation is the interference between reference pairs. With the accurate interference and blockage model mentioned, the following part gives the interference criteria which refers to threshold value R_B and main lobe θ' above. For better tractability, we formulate this resource allocation as an optimization problem while SINR precalculated as a metric utilized to measure the throughput. With certain constraints, we maximize throughput to achieve a more sensible scheme. As the total throughput, suffering from the interference, is a NP-hard problem, vertex coloring is assumed to settle the conflicts. By using vertex coloring, the flows which have conflicts during transmission are not in the same time slot.

D. INDOOR CONDITION

Utilizing Shannon capacity, the accessible transmission data rate is given by:

$$R_k = \alpha W_k \log_2(1 + SINR), \tag{24}$$

where α is the data rate loss during the transmission. As each link is independently distributed, the pass-loss exponent varies with receivers. For example, a NLOS link is desired and pass-loss is defined as α_N. The throughput of the network can be evaluated as:

$$R_{sum} = \sum_{k=1}^{n} R_k. \tag{25}$$

To further raise the throughput R_{sum}, the summation of R_k is maximized to achieve a superior allocation scheme. According to Eq. (25), we formulate the optimization problem as:

$$\max_{\{I_\phi\}} \sum_{k=1}^{n} R_k, \tag{26a}$$

$$\text{s.t. } SINR \geq \gamma, \tag{26b}$$

$$0 < k \leq n, \tag{26c}$$

$$\sum_{k=1}^{n} P_{r,k} = P_t G \left(\frac{\lambda}{4\pi}\right)^2 \left(\frac{1}{r}\right)^n \leq P_{\max}, \tag{26d}$$

$$\frac{R_k}{P_{r,k}} \geq \varepsilon \tag{26e}$$

where the constraint (26b) implies the received SINR must be greater than a threshold, and the constraint (26c) gives a power budget baseline. The constraint (26d) where $P_{r,k}$ is received power at user k, rules the fixed time slots since they are limited during propagation. In addition, the constraint (26e) enforces the proportion between achievable throughput and power assumption to be greater than an energy lower bound ε.

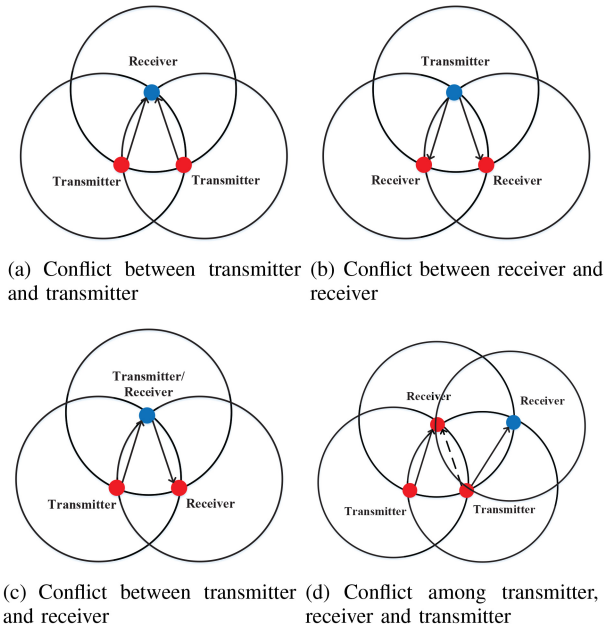

(a) Conflict between transmitter and transmitter (b) Conflict between receiver and receiver

(c) Conflict between transmitter and receiver (d) Conflict among transmitter, receiver and transmitter

FIGURE 7. Conflicts for indoor transmission.

It is clear that the optimization in Eq. (26) is a resource scheduling problem. The objective is to reduce interference when the threshold is satisfied. Thus, an interference graph is required to describe the situations for indoor scenarios. It is a typical vertex cover problem. In the mathematical discipline, a vertex cover problem can be formulated as a half-integral linear program which is one of Karp's 21 NP-hard problems. Owing to the complexity, we exploit the coloring vertex scheme to solve this problem. Before coloring, the indoor conflict conditions are required to be externalized in detail. During propagation, there are two kinds of conflicts defined, including primary conflict and secondary conflict. Apparently, when two links are from different directions, they could not be allocated in the same time-slot. In other words, the common node cannot transmit and receive simultaneously as shown in Fig. 7(c), which is known as primary conflict. As Fig. 7(d) shows, the interfering nodes confound the reference transmitters and receivers under a threshold range, called secondary conflict. To capture the characteristics of conflicts, the normalized main lobe pattern function is formulated as:

$$g(\theta') = \frac{G_{ff}(\theta')}{G_{\max}}. \tag{27}$$

According to this, being in beamwidth returns $g(\theta') = 1$; otherwise $g(\theta') = 0$ received. There are two conditions satisfied by the non-interfering simultaneous transmission: (1) whether the correlative receivers are in the beamwidth; (2) whether the correlative receivers are in the short-range of the threshold area being in beamwidth. Therefore, R_B is considered as the threshold value to judge whether g_i is a strong interference or not. While receivers are out the beamwidth $|g_k - g_i| \leq R_B$, g_i is a strong interference; otherwise not. However, a node locates in the beamwidth of the reference

transmitter, not within the range of R_B, and it still isn't an interference. As the interference criterion defined, there is a secondary conflict when the reference transmitter communicates with the reference receiver, facing strong interference within the beamwidth in the same slot.

Therefore, by exploiting the limited restrictions mentioned above, the $k \times k$ adjacency matrix due to indoor transmission situation could be achieved where k represents total active flows. Compared to the traditional serial scheme, concurrent transmission may suffer from the possible interference from other transmitters.

$$AdjacencyMatrix = \begin{bmatrix} 0 & 1 & 1 & 0 & 0 & 0 & 0 \\ 1 & 0 & 1 & 0 & 1 & 1 & 0 \\ 1 & 1 & 0 & 1 & 0 & 0 & 1 \\ 0 & 0 & 1 & 0 & 0 & 0 & 1 \\ 0 & 1 & 0 & 0 & 0 & 0 & 0 \\ 0 & 0 & 0 & 0 & 0 & 0 & 1 \\ 0 & 0 & 1 & 1 & 0 & 1 & 0 \end{bmatrix}. \quad (28)$$

From Eq. (28), the 7×7 adjacency matrix contains 1s and 0s and each row or column represents a flow where 1 implies a conflict. In addition, we could utilize the vertex coloring to allocate the time slot source to each transmitter when getting an adjacency matrix. In order to avoid interference and allocate time slots reasonably, the method of vertex coloring defines each vertex a flow and each color a resource block (time slot). If there is a conflict between two flows, we draw a line between the corresponding vertices. Based on the principle of minimum coloring, it colors neighbouring vertices (linked with each other) with different colors distinctly.

Accordingly, we utilize PVC algorithm based on maximum priority to allocate time slots, which means that the more edges a vertex has, the more preferentially it is colored. Convincingly, it is of the same basic principle as the indoor time slot allocation that a flow with more conflicts needs to be allocated with a high priority. Because of this characteristic, the weights do not demand recalculations. Thus, exploiting PVC scheme should highly according to the indoor resource blockage allocation.

E. OPTIMIZATION OF VERTEX COLORING ALGORITHM

However, the initial PVC Algorithm could even handle the conflicts among flows while the low efficiency still exists and actually became the bottleneck of the original approach. Because it is of high susceptibility that each time slot is allocated randomly. Therefore the allocation is full of uncertainty and randomness, so that not all time slots are active. That is to say, some time slots are allocated with more flows, increasing the probability of encountering more conflicts while some others are not. What is more, the time slot is a rare resource and requires to be fully utilized to maximize the throughput. Consequently, an optimization of the PVC Algorithm based on maximum priority is proposed.

As shown in Fig. 8, the vertex with the most edges is colored in priority. After coloring all the vertices, we add

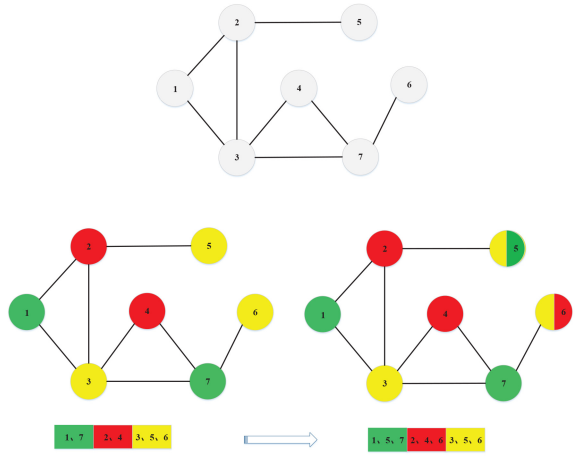

FIGURE 8. The schemes of PVC coloring and PMVC coloring are achieved by adjacency matrix.

Algorithm 1 PMVC Algorithm

Input:
Adjacency matrix G
Output:
Colored matrix V
$T = S \neq V$
while(T)
  $e = find(C == 1)$;
  $m = sum(G(m, :), 2)$
  $m(i) \geq m(i+1)$
  if $(color\_G = function\_colorV(i))$
    $V = \{v_i\}$;
    $Z = 1{:}n$;
    if $(f(V, Z) \neq 0$ too small)
      $t = find(G(f(V, Z), :) = 0)$;
      $color\_G = function\_colorV(t)$;
      $V_i = V_i \cup \{v\}$; $i = i + 1$
    else$(S = S \cup V_i)$
      $V_i = \{v\}$
    end if
  end if
end while
$b = size(find(G == i), 1)$;
$m1 = find(b == max(b)), m2 = find(b == min(b))$
for $(j = 1{:}n)$
  $kk = find(G(f, :) == 1), C(kk) = 0$
  $f = find(C == m2(1)), C(f) = 0$
  $y = find(C \neq 0)$,B(j+1,y)=m2
  if $(C == 0)$
    output V
  end if
end for

all rows of the adjacency matrix to judge the color which is least used and most used, respectively denoted as Min(k) and Max(k). Then, the vertices colored by Min(k) are required to be found next. We sort these least colored vertices by subscript and take the smallest one first. To capture the conflict conditions of the vertex, we define a new matrix C. With C, the vertex with Min(k) could be judged whether is propitious to be added with color Max(k). Afterwards, determine the new Min(k) and Max(k). When the number of each color returns to average, the algorithm terminates. The intrinsic principle of multiple coloring for a vertex is similar to the traditional PVC.

TABLE 1. Evaluation notations.

Parameter	Value
α_L	2
α_N	4
σ^2	-100
N, m, M	7, 0.125, 8
θ	$\frac{\pi}{6}$
P_t	1w

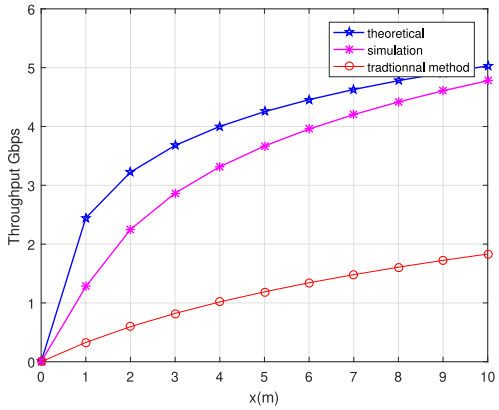

FIGURE 9. Theoretical throughput vs simulation throughput vs traditional Greedy method, which proves that PMVC scheme achieves more better throughput.

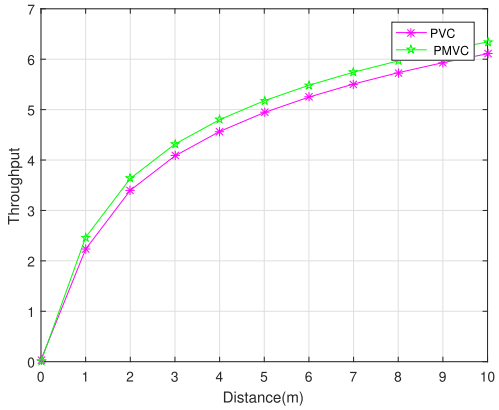

FIGURE 10. Throughput comparison between PMVC and PVC illustrates that the former scheme overmatches the later algorithm as the distance increases.

IV. NUMERICAL RESULTS

In this section, the comparison between greedy method and modified transmission allocation algorithms are provided. Table 1 lists parameter values used in the simulation.

To further validate the performance of the algorithm, with $PT = \lambda \log 2(1 + SINR)P_c\{SINR > \gamma\}$, the throughput is achieved by changing the distance from the reference transmitter to reference receiver. Fig. 9 shows that when the theoretical results are provided as a kind of reference, the method we have exploited is compared to the traditional greedy algorithm. It is clear that the performance in throughput of the greedy algorithm is far worse than the algorithm we proposed. The throughput we have obtained from PMVC scheme is closer to theoretical throughput. However, there is a huge gap between results from greedy and analytical throughput.

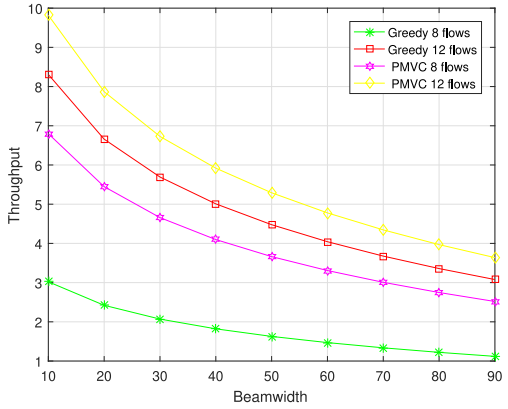

FIGURE 11. Throughput comparison between Greedy and PMVC when the number of flows equals to 8 and 12 respectively. As beamwidth increases, PMVC enables more flows to be transmitted in a time slot.

Besides, we evaluate PMVC Algorithm with increasing distance, to compare with PVC scheme. As shown in Fig. 10, PMVC is superior to PVC for PVC just has realized avoiding interference in the same time slot but would cause some time slots allocated with a large number of flows while the others did not. However, except for evading interference, PMVC scheme averages the flows in each slot, nearly leading to no difference in flow per slot. Thus, the variance is largely less than conventional greedy scheme. Then while beamwidth is studied, the total throughput of the active flows is given in Fig. 11. For indoor communication and resource block allocation, with the beamwidth increasing, it implies that the coverage of each signal has expanded along with the beamwidth's increase. Hence, the interference the reference transmitter would face is rising, resulting in the reduced chance that flows could be transmitted in the same time-slot. Under different flows, the throughput drops at different rates, which means the more flows there are, the much faster it descends.

Fig. 12 shows flow throughput per slot against the increasing number of active flows with beamwidth equal to 30 and 60 degrees. As flow numbers rise, the flow throughput per slot decreases. However, it can be seen that PMVC still provides better results than the Greedy algorithm. Accordingly, PMVC scheme can support more data transmission under the circumstance of the same flows. Because there are more flows allocated in the same slot as far as possible when we implement PMVC. Thus, the probability that resource block is allocated unevenly is reduced.

V. CONCLUSION

In this paper, we propose a system model to characterize objects and human bodies for indoor scenarios, integrating multi LOS ball with a self-blockage model. To better describe the characteristics of mmWave signal propagation, we assume the Nakagami fading to be independent of each kind of link, characterized by the path-loss exponent. A closed approximation expression of SINR can be given afterwards. The proposed model enables us to estimate system performance which shows good system

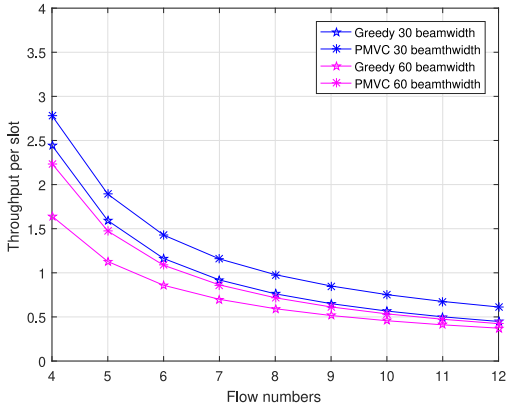

FIGURE 12. **Throughput per slot against flows when the beamwidth respectively equals to 30 and 60 degree. Also, the decline of rate means that the reference pairs are experiencing more conflicts.**

performance by comparing the simulation and analysis. When the interference and blockage model is determined, we discuss about the indoor transmission conditions. A maximum expression is given for capturing higher throughput, which leads to a NP-hard problem. To address this optimization problem, we propose a PMVC algorithm to enhance the system throughput, reducing the interference simultaneously. Compared with traditional Greedy algorithm and PVC scheme, the PMVC we proposed achieves much better performance in throughput.

For future work, we can consider the times that the mmWave reflects from the walls and ceiling and define the intensity of the transmission link according to the times. It will help us further explore the relations between strong and weak interferers. Meanwhile, we are supposed to take the effects of back lobes into account.

REFERENCES

[1] B. Ma, H. Shah-Mansouri, and V. W. S. Wong, "Multimedia content delivery in millimeter wave home networks," *IEEE Trans. Wireless Commun.*, vol. 15, no. 7, pp. 4826–4838, Jul. 2016.

[2] Y. Hao, Y. Miao, L. Hu, M. Hossain, G. Muhammad, and S. Amin, "Smart-edge-CoCaCo: AI-enabled smart edge with joint computation, caching, and communication in heterogeneous IoT," *IEEE Netw.*, vol. 33, no. 2, pp. 58–64, Mar./Apr. 2019.

[3] A. Zhang, J. Chen, R. Hu, and Y. Qian, "SeDS: Secure data sharing strategy for D2D communication in LTE-advanced networks," *IEEE Trans. Veh. Technol.*, vol. 65, no. 4, pp. 2659–2672, Apr. 2016.

[4] D. Wu, J. Wang, R. Q. Hu, Y. Cai, and L. Zhou, "Energy-efficient resource sharing for mobile device-to-device multimedia communications," *IEEE Trans. Veh. Technol.*, vol. 63, no. 5, pp. 2093–2103, Jun. 2014.

[5] D. Wu, L. Zhou, Y. Cai, R. Q. Hu, and Y. Qian, "The role of mobility for D2D communications in LTE-advanced networks: Energy vs. bandwidth-efficiency," *IEEE Wireless Commun. Mag.*, vol. 21, no. 2, pp. 66–71, Apr. 2014.

[6] L. Zhou, R. Q. Hu, Y. Qian, and H.-H. Chen, "Energy-spectrum efficiency tradeoff for video streaming over mobile ad hoc networks," *IEEE J. Sel. Areas Commun.*, vol. 31, no. 5, pp. 981–991, May 2013.

[7] L. Zhou, "Mobile Device-to-device video distribution: Theory and application," *ACM Trans. Multimedia Comput. Commun. Appl.*, vol. 12, no. 3, pp. 1253–1271, 2015.

[8] L. Zhou, D. Wu, J. Chen, and Z. Dong, "Greening the smart cities: Energy-efficient massive content delivery via D2D communications," *IEEE Trans. Ind. Informat.*, vol. 14, no. 4, pp. 1626–1634, Apr. 2018.

[9] P. Liu, M. Di Renzo, and A. Springer, "Line-of-sight spatial modulation for indoor mmWave communication at 60 GHz," *IEEE Trans. Wireless Commun.*, vol. 15, no. 11, pp. 7373–7389, Nov. 2016.

[10] T. Bai and R. W. Heath, "Coverage and rate analysis for millimeter-wave cellular networks," *IEEE Trans. Wireless Commun.*, vol. 14, no. 2, pp. 1100–1114, Feb. 2015.

[11] M. D. Renzo, "Computational stochastic geometry—on system-level modeling, simulation, performance evaluation, optimization, and experimental validation of 5G wireless communication networks," in *Proc. Int. Conf. Commun. Manag. Telecommun. (ComManTel)*, Da Nang, Vietnam, 2015, pp. 1–2.

[12] A. F. Darwesh and A. O. Fapojuwo, "Secrecy rate analysis of mmWave MISO ad hoc networks with null space precoding," in *Proc. IEEE Wireless Commun. Netw. Conf. (WCNC)*, 2020, pp. 1–6.

[13] M. Di Renzo, "Stochastic geometry modeling and analysis of multi-tier millimeter wave cellular networks," *IEEE Trans. Wireless Commun.*, vol. 14, no. 9, pp. 5038–5057, Sep. 2015.

[14] A. Thornburg, T. Bai, and R. W. Heath, "Performance analysis of outdoor mmWave ad hoc networks," *IEEE Trans. Signal Process.*, vol. 64, no. 15, pp. 4065–4079, Aug. 2016.

[15] T. Bai and R. W. Heath, "Analysis of self-body blocking effects in millimeter wave cellular networks," in *Proc. 48th Asilomar Conf. Signals Syst. Comput.*, Pacific Grove, CA, USA, 2014, pp. 1921–1925.

[16] M. Zarifneshat, P. Roy, and L. Xiao, "Multi-objective approach for user association to improve load balancing and blockage in millimeter wave cellular networks," *IEEE Trans. Mobile Comput.*, early access, Oct. 37, 2021, doi: 10.1109/TMC.2021.3122972.

[17] M. Di Renzo, "Stochastic geometry modeling and performance evaluation of mmWave cellular communications," in *Proc. IEEE Int. Conf. Commun. (ICC)*, London, U.K., 2015, pp. 5992–5997.

[18] X. Pang, J. Tang, N. Zhao, X. Zhang, and Y. Qian, "Energy-efficient design for mmWave-enabled NOMA-UAV networks," *Sci. China Inf. Sci.*, vol. 64, no. 4, pp. 1–14, 2021.

[19] O. Yazdani, M. Monemi, and G. Mirjalily, "Fast globally optimal transmit antenna selection and resource allocation scheme in mmWave D2D networks," *IEEE Trans. Mobile Comput.*, vol. 21, no. 2, pp. 573–584, Feb. 2022.

[20] X. Zhong, Y. Guo, N. Li, and Y. Chen, "Joint optimization of relay deployment, channel allocation, and relay assignment for UAVs-aided D2D networks," *IEEE/ACM Trans. Netw.*, vol. 28, no. 2, pp. 804–817, Apr. 2020.

[21] X. Wang *et al.*, "Millimeter wave communication: A comprehensive survey," *IEEE Commun. Surveys Tuts.*, vol. 20, no. 3, pp. 1616–1653, 3rd Quart., 2018.

[22] K. Venugopal, M. C. Valenti, and R. W. Heath, "Analysis of millimeter wave networked wearables in crowded environments," in *Proc. 49th Asilomar Conf. Signals Syst. Comput.*, Pacific Grove, CA, USA, 2015, pp. 872–876.

[23] G. George, K. Venugopal, A. Lozano, and R. W. Heath, "Enclosed mmWave wearable networks: Feasibility and performance," *IEEE Trans. Wireless Commun.*, vol. 16, no. 4, pp. 2300–2313, Apr. 2017.

[24] K. Venugopal and R. W. Heath, "Location based performance model for indoor mmWave wearable communication," in *Proc. IEEE Int. Conf. Commun. (ICC)*, Kuala Lumpur, Malaysia, 2016, pp. 1–6.

[25] Y. Li, Z. Guo, T. Yang, L. Jiang, and M. Li, "Satisfied matching-embedded social Internet of Things for content preference-aware resource allocation in D2D underlaying cellular networks," *IEEE Internet Things J.*, early access, Sep. 21, 2021, doi: 10.1109/JIOT.2021.3113914.

[26] W. ur Rehman, T. Salam, and X. Tao, "Vertex multi-coloring scheduling algorithm for concurrent transmission in 60-GHz networks," in *Proc. IEEE Global Commun. Conf.*, Austin, TX, USA, 2014, pp. 4751–4757.

[27] Y. Zhu, G. Zheng, L. Wang, K. Wong, and L. Zhao, "Content placement in cache-enabled sub-6 GHz and millimeter-wave multi-antenna dense small cell networks," *IEEE Trans. Wireless Commun.*, vol. 17, no. 5, pp. 2843–2856, May 2018.

[28] M. Abouelseoud and G. Charlton, "The effect of human blockage on the performance of millimeter-wave access link for outdoor coverage," in *Proc. IEEE 77th Veh. Technol. Conf. (VTC Spring)*, Dresden, Germany, 2013, pp. 1–5.

[29] M. Chen, L. Wang, J. Chen, X. Wei, and L. Lei, "A computing and content delivery network in the smart city: Scenario, framework, and analysis," *IEEE Network*, vol. 33, no. 2, pp. 89–95, Mar./Apr. 2019.

[30] C. Huang, L. Liu, C. Yuen, and S. Sun, "Iterative channel estimation using LSE and sparse message passing for mmWave MIMO systems," *IEEE Trans. Signal Process.*, vol. 67, no. 1, pp. 245–259, Jan. 2019.

[31] C. Huang, A. Zappone, G. Alexandropoulos, M. Debbah, and C. Yuen, "Reconfigurable intelligent surfaces for energy efficiency in wireless communication," *IEEE Trans. Wireless Commun.*, vol. 18, no. 8, pp. 4157–4170, Aug. 2019.